Giordano, R. M., and J. C. Slattery, "Interfacial Effects Upon Displacement in Sinusoidal Capillaries," *AIChE Symp. Ser.*, **78**, 58 (1982).
Lessen, M., and P.-S. Huang, "Poiseuille Flow in a Pipe with Axially Symmetric Wavy Walls," *Phys. Fluids*, **19**, 945 (1976).
Neira, M., and A. C. Payatakes, "Collocation Solution of Creeping Newtonian Flow Through Periodically Constricted Tubes with Piecewise Continuous Wall Profile," *AIChE J.*, **24**, 42 (1978).
Neira, M., and A. C. Payatakes, "Collocation Solution of Creeping Newtonian Flow Through Sinusoidal Tubes," *AIChE J.*, **25**, 725 (1979).
Oh, S. G., and J. C. Slattery, "Interfacial Tension Required for Significant Displacement of Residual Oil," *Soc. Petrol. Eng. J.*, **19** (1979).
Payatakes, A. C., Chi Tien, and R. M. Turian, "A New Model for Granular Porous Media, Part I. Model Formulation," *AIChE J.*, **19**, 58 (1973a).
Payatakes, A. C., Chi Tien, and R. M. Turian, "Part II. Numerical Solution of Steady State Incompressible Newtonian Flow Through Periodically Constricted Tubes," *AIChE J.*, **19**, 67 (1973b).
Payatakes, A. C., Chi Tien, and R. M. Turian, "Further Work on the Flow Through Periodically Constricted Tubes—A Reply," *AIChE J.*, **19**, 1036 (1973c).
Payatakes, A. C., Chi Tien, and R. M. Turian, "Trajectory Calculation of Particle Deposition in Deep Bed Filtration, Part I. Model Formulation," *AIChE J.*, **20**, 889 (1974a).
Payatakes, A. C., Chi Tien, and R. M. Turian, "Part II. Case Study of the Effect of Dimensionless Groups and Comparison with Experimental Data," *AIChE J.*, **20**, 900 (1974b).
Payatakes, A. C., K. M. Ng, and R. W. Flumerfelt, "Oil Ganglion Dynamics During Immiscible Displacement—Model Formulation," *AIChE J.*, **26**, 430 (1980).
Sheffield, R. E., and A. B. Metzner, "Flow of Nonlinear Fluids Through Porous Media," *AIChE J.*, **22**, 736 (1976).
Slattery, J. C., "Interfacial Effects on the Entrapment and Displacement of Residual Oil," *AIChE J.*, **20**, 1145 (1974).
Tien, Chi, and A. C. Payatakes, "Advances in Deep Bed Filtration," *AIChE J.*, **25**, 737 (1979).

Kinetics of the Self-Fouling Oxidation of Hydrogen Sulfide on Activated Carbon

PAN ZHENGLU, HUNG-SHAN WENG, FENG HAN-YU, and J. M. SMITH

Department of Chemical Engineering
University of California
Davis, CA 95616

Most of the prior investigations of the catalytic reaction (on activated carbon)

$$H_2S(g) + \tfrac{1}{2}O_2(g) \rightarrow H_2O(g) + S \qquad (1)$$

have used thermal gravity apparatus, determining the rate from the weight of deposited sulfur. Steijins et al. (1976) reported that the sulfur product deposited on the carbon had some catalytic activity. Coskun and Tollefson (1977) noted that the rate of the reaction decreased with time, presumably due to sulfur deposition. Sreeramamurthy and Menon (1975) found that sulfur powder alone did not show catalytic activity. However, there has not been agreement about the kinetics of the reaction. For example, Cariaso and Walker (1975) concluded that the rate was first order in hydrogen sulfide and zero order in oxygen. Coskun and Tollefson proposed one-half order with respect to hydrogen sulfide, and Steijns et al suggested an oxidation-reduction mechanism. Also quantitative rate equations have not been presented.

Our objectives were first to measure reaction rates on fresh activated carbon, and then to determine the effect of deposited sulfur product. Data were obtained for the fresh catalyst in an isothermal, fixed-bed, differential reactor. The concentration range studied was about 1 to 10% for both hydrogen sulfide and for oxygen; measurements were made at 313 K to 353 K and at 108 kPa. For these conditions no sulfur dioxide is produced; the only products are solid sulfur and water vapor. Most of the deactivation measurements were carried out at 323 K over a time interval of 0 to 780 s. At longer times the rate decreases very slowly. Coskun and Tollefson (1977) found that the only products of the reaction on activated carbon, at temperatures below 473 K, were water and sulfur. Cariaso and Walker (1975) showed that deposited sulfur is not measurably oxidized to sulfur dioxide at temperatures below 413 K. In our chromatographic analyses of the effluent gas we found no other peaks than those for N_2, O_2, H_2S and H_2O. Hence, for our studies with a maximum temperature of 353 K, it was assumed that the only reaction was Eq. 1.

P. Zhenglu is on leave from Tianjin Research Institute of Petrol-Chemical Industry, Tianjin, China; H. Weng, from Cheng Kung University, Tainan, China; and F. Han-Yu, from Gansu Teachers University, Lanzhou, China.

EXPERIMENTAL

The range of flow rates and other operating conditions are summarized in Table 1.

Apparatus

The Pyrex reactor (0.01 m I.D.) is shown with dimensions in Figure 1. The activated-carbon catalyst bed was held in the downflow reactor with a fritted disk. Both the Pyrex reactor and stainless-steel preheater coil (0.0317 m I.D., 2.29 m length) were immersed in a constant temperature bath. Figure 2 is a schematic diagram of the apparatus. Mixtures of oxygen, hydrogen sulfide, and nitrogen were prepared in feed tanks 1 and 2. The temperature was measured with an iron-constantan thermocouple inserted in the middle of the bed. The maximum temperature difference between bath and catalyst bed was 3 K. The catalyst charge was about 1×10^{-4} kg. For runs made with water vapor the gas mixture from the feed tank was passed through a saturator operated at a controlled, constant temperature.

Chemicals

The catalyst was a coal-based activated carbon, type BPL from Pittsburgh Activated Carbon Company. It is a high sulface area, broad pore-size distribution material whose properties are given in Table 2. Granular particles with an average diameter of 0.398×10^{-3} m (32–48 mesh) were used in the catalyst beds. Before use the particles were blown with air to remove fines and degassed with N_2.

TABLE 1. OPERATING CONDITIONS FOR FRESH CATALYST RUNS

Temperature	313 to 353 K
Pressure	108.1 kPa
H_2S Concentration (Avg.)[a]	0.41 to 4.35×10^{-3} kmol/m^3
O_2 Concentration (Avg.)[a]	0.11 to 4.07×10^{-3} kmol/m^3
H_2O Concentration (Feed)[a]	0 to 0.5×10^{-3} kmol/m^3
Conversion Range of H_2S	0.03 to 0.26
Flow Rate of Feed Gas[a]	2.5×10^{-6} m^3/s (at 298 K, 101.3 kPa)

[a] Measured at 298 K and 101.3 kPa.

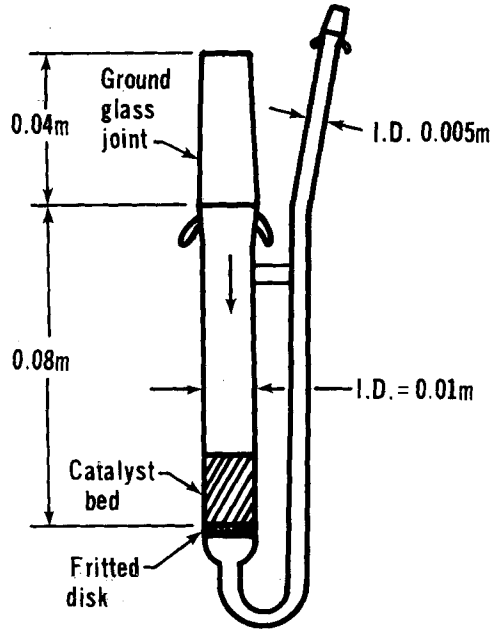

Fig. 1. Diagram of reactor.

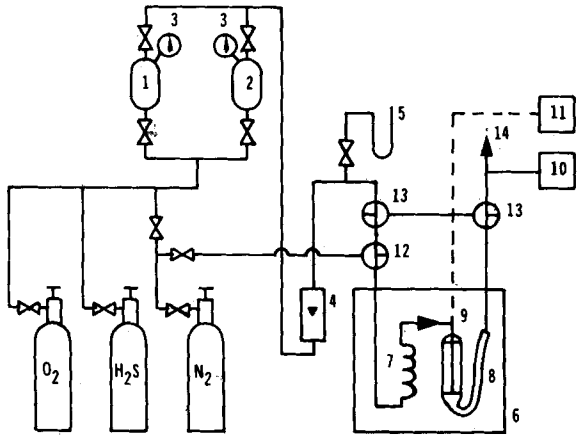

Fig. 2. Schematic diagram of apparatus [1, 2, gas mixture feed tanks; 3, pressure gauges; 4, rotameter; 5 manometer; 6, thermostat; 7, preheater; 8, reactor; 9, thermocouple; 10, chromatograph; 11, recorder; 12, 13, 3-way valves; 14, exhaust line].

The Matheson Company hydrogen sulfide had a stated purity of not less than 99%. The oxygen (Matheson) used contained less than 0.5 ppm of total hydrocarbons and less than 50 ppm of nitrogen. The nitrogen purity was 99.7%.

Analysis

The feed and exit gases from the reactor were analyzed for hydrogen sulfide and for oxygen in a gas chromatograph (Varian Aerograph Co., Model 1400) operating at the following conditions: column temperature = 406 K; thermal conductivity detector temperature = 413 K; carrier gas (He) flow rate = 0.5×10^{-6} m^3/s; Porapak N column for hydrogen sulfide and 5A molecular sieve column for oxygen, both 1.64 m long.

Pore-Volume Distribution

The effect of deposited sulfur on the pore-volume distribution of the activated carbon was also measured. A 60,000 psi (413 MPa) mercury porosimeter (American Instrument Co.) was used for pore diameters from 12×10^{-6} to 3×10^{-9} m and nitrogen desorption for smaller pores. For the latter measurements the amount of nitrogen condensed (at liquid nitrogen temperature) in the pores of a sample of activated carbon was determined by warming the sample and measuring the desorbed nitrogen. From runs made with different compositions of nitrogen and helium, the amount of nitrogen condensed at different pressures could be obtained. From these data, a pore volume vs. pore diameter curve was constructed using the modified Kelvin equation (Smith, 1981).

Table 2. Properties of Activated Carbon

Total Surface Area[a] (N_2, BET Method)	1.050 to 1.150×10^6 m^2/kg
Particle Density[a] (Hg Displacement)	800 to 850 kg/m^3
True Density[a] (He Displacement)	2,100 kg/m^3
Pore Volume[a] (within Particles)	7 to 8×10^{-4} m^3/kg
Void Fraction in Catalyst Bed	0.40–0.43
Avg. Particle Size (32–48 mesh) (Effect of particle size determined from data covering a particle size range 0.275 to 2.05×10^{-3} m.)	0.398×10^{-3} m

[a] From Pittsburgh Activated Carbon Co.

RESULTS FOR FRESH CATALYST

Reaction rates were measured for the fresh catalyst as a function of gas composition and temperature. Also rates were determined as a function of time at 50°C for constant gas concentrations of hydrogen sulfide and oxygen, each equal to 1.11×10^{-3} kmol/m^3. The results for the fresh catalyst are analyzed first and then the deactivation data are considered.

The catalyst suffers a significant decrease in rate in the first few minutes of use. Hence, it is important to analyze the effluent gas at the same time for all runs with the "fresh" catalyst. In our apparatus the average residence time from the three-way feed valve (Figure 2) to the gas chromatograph sampling valve was 45 s. Some mixing occurs in this volume. By trial it was found that data taken 60 s after turning the three-way feed valve gave the most reproducible results. Hence, zero time for the deactivation data is at this 60 s time and the fresh catalyst results also apply at this time.

The reaction rate was calculated from the feed and exit hydrogen sulfide concentrations, using the differential-reactor equation

$$r_{H_2S} = \frac{(C_f - C_o)_{H_2S}}{w} Q \qquad (2)$$

where the flow rate Q and concentrations are both evaluated at 298 K and 101.3 kPa. Since both concentrations and conversion are low, the volumetric flow rate through the reactor does not change significantly due to the change in number of moles due to reaction. The effluent flow rate was used in Eq. 2.

Experimental Data

Illustrative results for the effect of oxygen and hydrogen sulfide concentrations on the rate are shown by the data points in Figures 3 and 4. Reproducibility of the data is indicated by the multiple points at the same concentration. The rate first increases with C_{O_2} but then becomes zero order (Figure 3), while the rate continues to increase with C_{H_2S}. The concentrations used are the average of the feed and exit values. An Arrhenius plot at constant concentrations of rate data from 313 to 353 K indicated an apparent activation energy of 13×10^3 kJ/kmol. Coskun and Tollefson (1977) and Cariaso and Walker (1975) also found low values, $21–26 \times 10^3$ kJ/kmol.

To determine if water vapor, a reaction product, affected the rate, data were obtained at 323 K when water vapor was added to the feed. Up to a maximum concentration more than twice the level that could be obtained from the rate of reaction, no significant effect was observed.

At 323 K and constant concentrations, rate values for four particle sizes, up to 2×10^{-3} m (7–14 mesh), showed no significant change. Hence, the kinetics data, for which particles with a diameter of 0.275×10^{-3} m were used, are supposed not to involve intraparticle transport resistances.

The effect of gas-to-particle mass transfer was estimated by

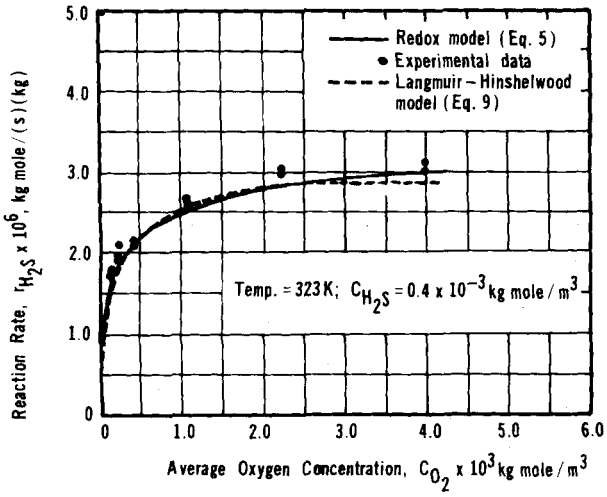

Fig. 3. Calculated and experimental rates at constant H_2S concentration.

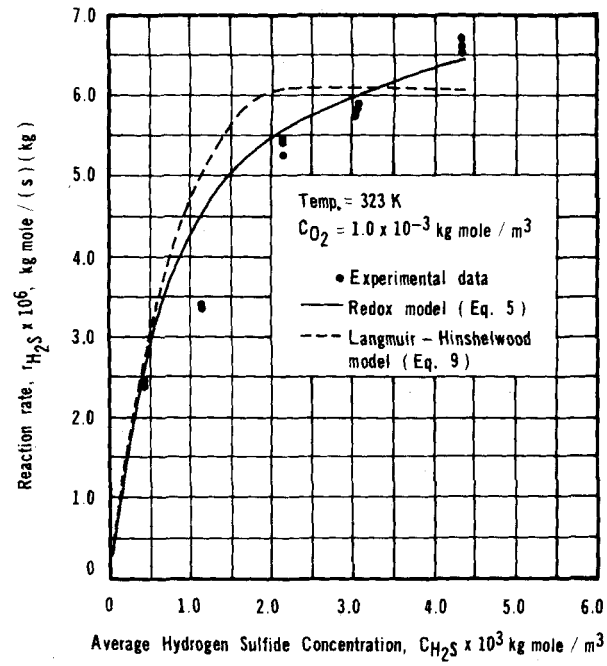

Fig. 4. Calculated and experimental rates at constant O_2 concentration.

calculating the mass transfer coefficient k_m from the correlation of Dwivedi and Upadhay (1977). Using this result and the highest observed reaction rate, 6.6×10^{-6} kmol/(s)(kg activated carbon), the concentration ratio $(C_b - C_s)/C_b$ for hydrogen sulfide is only 0.01. Hence, external mass transport is not significant, and the observed rates should represent intrinsic kinetics.

Fresh Catalyst Rate Equation

Several proposals have been made for the mechanism of the reaction of Eq. 1, but apparently no quantitative rate equations have been published. Our data are not of a type to establish a mechanism, but numerical equations for the rate can be established. We have analyzed the rate data with two general types of expressions. The first is a redox-type equation. Such formulations have been often used for correlating oxidation rates (Mars and van Krevelen, 1949; Cappelli, 1975). An irreversible adsorption of dissociated oxygen followed by production of adsorbed sulfur is assumed:

$$O_2(g) + 2X \xrightarrow{k_1} 2O{\cdot}X \tag{3}$$

$$O{\cdot}X + H_2S(g) \xrightarrow{k_2} S{\cdot}X + H_2O(g) \tag{4}$$

By equating rates of the oxidation and reduction steps, the resulting expression is

$$r_{H_2S} = \frac{k_1 k_2 C_{O_2}^{1/2} C_{H_2S}}{k_1 C_{O_2}^{1/2} + k_2 C_{H_2S}} = \frac{2.23 \times 10^{-6}\, C_{O_2}^{1/2} C_{H_2S}}{2.35 \times 10^{-4} C_{O_2} + 9.48 \times 10^{-3}\, C_{H_2S}} \tag{5}$$

where numerical form represents our data at 323 K.

A second type of expression can be derived, from a number of mechanisms, using the Langmuir-Hinshelwood approach with the surface-reaction step assumed to control the rate. For example, both oxygen and hydrogen sulfide may be absorbed and surface reaction occurs between the adsorbed species, according to the three-step mechanism

$$^1/_2O_2(g) + X \underset{k_3'}{\overset{k_3}{\rightleftharpoons}} O{\cdot}X \tag{6}$$

$$H_2S(g) + X \underset{k_4'}{\overset{k_4}{\rightleftharpoons}} H_2S{\cdot}X \tag{7}$$

$$H_2S{\cdot}X + O{\cdot}X \xrightarrow{k_5} H_2O(g) + S{\cdot}X + X \tag{8}$$

Other mechanisms leading to the same functional form of the concentrations involve absorbed water or an adsorbed species $H_2S{\cdot}O{\cdot}X$. The rate equation from Eqs. 6–8 is

$$r_{H_2S} = \frac{k_5 K_3 K_4 C_{O_2}^{1/2} C_{H_2S}}{(1 + K_3 C_{O_2}^{1/2} + K_4 C_{H_2S})^2} = \frac{0.70 C_{O_2}^{1/2} C_{H_2S}}{(1 + 20 C_{O_2}^{1/2} + 5.5 \times 10^2 C_{H_2S})^2} \tag{9}$$

where again the numerical form is for 323 K. Here K_3 and K_4 are adsorption equilibrium constants for reversible reactions 6 and 7.

All of the rate data were used with linear regression analysis to establish the numerical values of the constants shown in Eqs. 5 and 9. The fit of the equations is illustrated in Figures 3 and 4 for some of the data at 323 K. The redox model fits the data best, not only at the conditions of Figures 3 and 4 but for all the rate data. Also, it can be written in a form with but two constants instead of the three constants in the Langmuir-Hinshelwood formulation. Hence, the redox form is preferred for the conditions of our experiments.

DEACTIVATION KINETICS

Figure 5 shows how the observed reaction rate decreases with time at 323 K and for constant feed concentrations of hydrogen sulfide and oxygen. The values shown at zero time are for samples taken for analysis 60 s after the three-way feed valve had admitted reaction gases to the system. Two measurements were made at each time. The amount of sulfur deposited on the carbon can be calculated by integrating the rate data with respect to time. The results are shown in Figure 6 where one curve gives the weight of sulfur deposited per unit weight of activated carbon, and the other curve represents the fraction of the carbon surface covered by sulfur. This fraction was calculated from the weight of sulfur deposited by assuming that sulfur is adsorbable in a monolayer on all of the sites that are determined by nitrogen absorption and that the projected area of the sulfur atom is 9.71×10^{-20} m^2.

Comparing the data in Figures 5 and 6 indicates that the small sulfur deposit (3.2% of the weight of the carbon) at 780 s causes a four-fold decrease in reaction rate. Also, on a monolayer basis, and even allowing for some uncertainty in the area of the deposited sulfur atom, less than 5% of the carbon surface is occupied by sulfur. The absence of intraparticle diffusion resistance shown by the rate data for different particle sizes suggests that pore-mouth poisoning

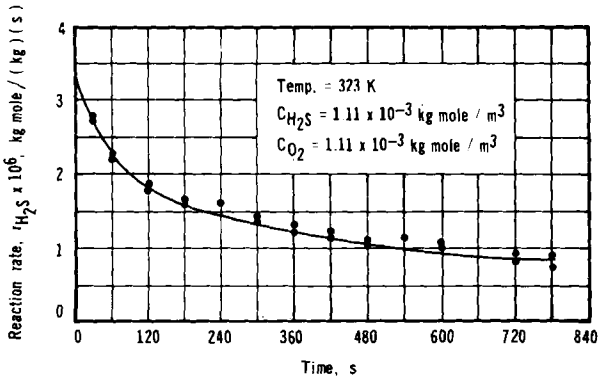

Fig. 5. Reaction rate vs. time.

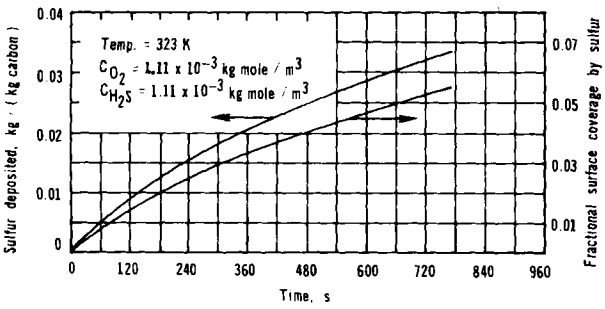

Fig. 6. Deposited sulfur vs. reaction time.

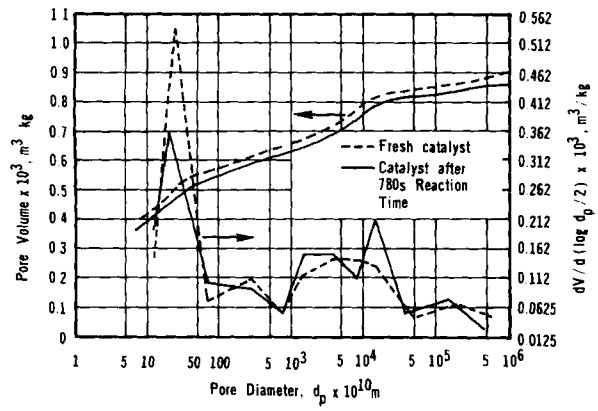

Fig. 7. Pore Volume of fresh and used activated carbon.

is not occurring, so that deactivation occurs uniformly throughout the particles.

Figure 5 shows that the rate decreases very rapidly during the first 120 s but falls very slowly after 600 s. In long-time runs (up to 3 days) the rate did not approach a constant value but continued to decrease very slowly with time. This behavior cannot be explained by a linear deactivation function, based upon complete poisoning of the carbon sites occupied by sulfur. This proposal would lead to an exponential curve of rate vs. time, with an asymptotic rate of zero, which does not fit the data, for example, as seen in Figure 5. The very slow decay at long times indicates that the deposited sulfur has some activity for the reaction. Based upon their experimental observations, Steijns et al. (1976) suggested the same result that the reaction was autocatalytic. However, sulfur powder alone was found not to be an active catalyst (Sreeramamurthy and Menon, 1975).

Our deactivation data can be explained quantitatively by supposing that sulfur has an intrinsic catalytic activity about one-fourth as large as that of activated carbon. However, it is necessary to base the derived equations on no interaction between activated carbon and the deposited sulfur. That is, it is necessary to assume that the sulfur and carbon sites each catalyze the reaction independently and also that the two rates are each proportional to their respective surfaces. These assumptions are untested so that inclusion of a quantitative treatment here seems unjustified. What is clear is that the rate behavior cannot be reasonably explained solely by deactivation of the carbon sites. Further, the small sulfur deposit (3.2 wt. % at 780 s) does not cause a significant change in the pore structure of the carbon. Figure 7 shows the measured pore-volume distribution for fresh carbon and that subjected to 780 s reaction time. Neither the distribution nor cumulative pore volume are significantly different for the two catalysts. In conclusion, all that can be stated at this time is that deposited sulfur, in some unknown way, reduces but does not completely deactivate (until complete pore blockage occurs) the activated carbon catalyst.

ACKNOWLEDGMENT

The financial assistance of National Science Foundation Grant CPE-8025831 is gratefully acknowledged. Also we thank the National Science Council (Taiwan, China) and the Chinese ministry of Education for fellowship support.

NOTATION

A = parameter, equal to $(r_C)_o/q_o$, s^{-1}
C_{H_2S} = average intraparticle or bulk concentration of H_2S in reactor, kmol/m^3
C_{O_2} = average intraparticle or bulk concentration of O_2 in reactor, kmol/m^3
C_f, C_o = feed and effluent concentrations to and from reactor, kmol/m^3
C_b, C_s = bulk and surface concentrations, kmol/m^3
d_p = equivalent cylindrical pore diameter, m
k_1, k_2 = reaction rate constants, in redox rate expression, Eq. 5
$k_3, k_3', k_4, k_4', k_5$ = rate constants in Langmuir-Hinshelwood rate expression. Eq. 9
Q = volumetric gas flow rate (at 298 K and 101.3 kPa), m^3/s
q = concentration of carbon sites poisoned by sulfur; q_o = total concentration of active sites, kmol/(kg carbon)
r = rate of reaction, kmol H_2S/(kg carbon)(s)
r_C = rate of reaction on activated carbon sites, kmol/(kg carbon)(s); $(r_C)_o$ = rate on fresh carbon
r_S = rate of reaction on sites occupied by sulfur, kmol/(kg carbon)(s); $(r_S)_o$ = rate when all active sites of carbon are occupied by sulfur; kmol/(kg carbon)(s)
t = on-stream reaction time, s
w = mass of activated carbon in reactor, kg

Greek Letter

ϕ = fraction of active carbon sites occupied by sulfur

LITERATURE CITED

Cappelli, A., "Chemical Reaction Engineering Reviews," *Adv. Chem. Ser.*, **148**, 212, Amer. Chem. Soc., Washington, DC (1975).
Cariaso, O. C., and P. L. Walker, Jr., "Oxidation of Hydrogen Sulfide over Microporous Carbons," *Carbon*, **13**, 233 (1975).
Coskun, I., and E. L. Tollefson, "Oxidation of Low Concentrations of Hydrogen Sulfide over Activated Carbon," *5th Can. Symp. Catal.*, 469, Chem. Inst. Can., Ottawa, Ont. (1977).
Dwivedi, P. N., and S. N. Upadhay, "Particle-Fluid Mass Transfer in Fixed and Fluidized Beds," *Ind. Eng. Chem. Proc. Des. Dev.*, **16**, 157 (1977).

Mars, P., and D. W. van Krevelen, "Oxidation-Reduction Catalytic Reactions," *Chem. Eng. Sci. Special Suppl.*, 3, 41 (1949).
Smith, J. M., *Chemical Engineering Kinetics*, 3rd Ed., 343, McGraw-Hill, New York (1981).
Sreeramamurthy, R., and P. G. Menon, "Oxidation of H_2S on Active Carbon Catalyst," *J of Cat.*, 37, 287 (1975).
Steijns, M., F. Derks, A. Verloop, and P. Mars, "The Mechanism of the Catalytic Oxidation of Hydrogen Sulfide. II: Kinetics and Mechanism of Hydrogen Sulfide Oxidation Catalyzed by Sulfur," *J. of Cat.*, 42, 87 (1976).

Manuscript received April 19, 1983; revision received June 3, and accepted June 23, 1983.

Mechanistic Models for Transitions between Regimes of Fluidization

WEN-CHING YANG

Research and Development Center
Westinghouse Electric Corporation
Pittsburgh, PA 15235

INTRODUCTION

Understanding the flow regime transitions is important because different flow regimes provide vastly different solid circulation patterns, solids and gas mixing rates, and thus the chemical reaction rates. They, in turn, dictate the reactor design considerations. There are very few theoretical discussions and correlations available in the literature on the criteria of flow transitions between these different regimes. This paper attempts to develop mechanistic models to predict these flow transitions for fine particles generally belonging to Geldart's Class A (1973).

GENERAL FLUIDIZATION REGIME DIAGRAM

A qualitative fluidization map for fine particles was initially proposed by Yerushalmi et al. (1978) and refined later in Yerushalmi and Cankurt (1979). A more recent and more general fluidization regime diagram was presented by Li and Kwauk (1980), Figure 1. The log-log coordinates are used here, instead of the original semilogarithmic presentation, to show the approximately straight-line relationship in different regimes, which will become more apparent later. Use of the voidage as the ordinate and the gas velocity as the abscissa allows a convenient presentation for fluidization regimes from incipient fluidization all the way to dilute-phase pneumatic transport. Different fluidization regimes simply exhibit different voidage-gas velocity relations.

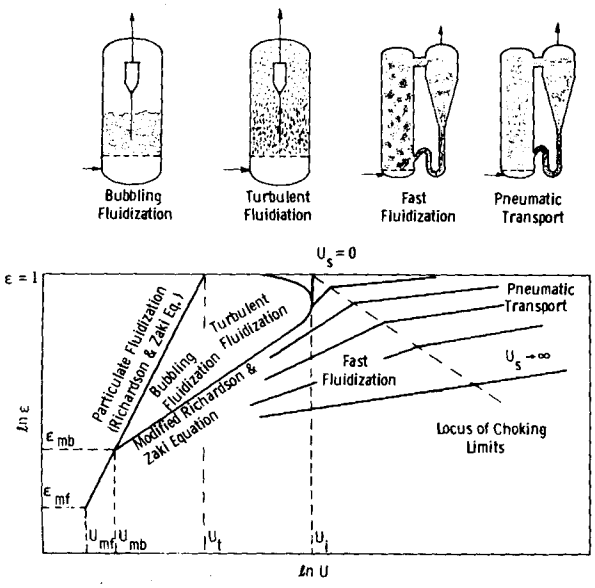

Figure 1. Schematic fluidization regime diagram (Li and Kwauk, 1980).

THEORY OF CLUSTER FORMATION

The application of the concept of cluster formation was first suggested by Yerushalmi et al. (1978). Matsen (1982) also used it in his analysis of choking and entrainment mechanisms. A quantitative theory, however, was first proposed by Capes (1974) for application to the fluidization of fine particles. He followed the development of the concept of flocs during sedimentation by Scott (1968) and modified the Richardson and Zaki equation (1954) to include an "effective" porosity, as shown in Eq. 1.

$$\frac{U}{U_i} = \epsilon_e^m = (1 - KC)^m. \tag{1}$$

The "effective" porosity, ϵ_e, includes the void space between aggregates (or clusters) only while ϵ, the apparent voidage, includes also the void space between solid particles inside the clusters. He attributed the large values of n in the Richardson and Zaki equation often reported in the literature for fine particles (ranging up to a value of 10) to the increased effective particle volume caused by agglomeration or to the irregular particle shape, which immobilized a layer of fluid in the surface irregularities. Using Eq. 1 with the "effective" voidage brings the exponent m within the range of the original Richardson and Zaki equation.

The bed density reported by Yerushalmi and Cankurt (1979) and the voidage-gas velocity relation reported by Li and Kwauk (1980) were processed to give the best fit using the original Richardson and Zaki equation and the modified one shown in Eq. 1. The results are summarized in Table 1. The U_i can be considered to be the terminal velocity of a cluster with the "effective" particle diameter. In fitting Eq. 1 to the experimental data, the procedure Capes (1974) suggested was followed. The calculation was carried out until the value of m and n agreed to within 0.02. The successful correlation of these experimental data indicates that, hydrodynamically, these fluid beds are similar to beds with "clusters" of finite sizes.

CONTINUITY WAVE AND TRANSITION FROM BUBBLING TO TURBULENT FLUIDIZATION

The continuity wave exists as a quasisteady-state phenomenon whenever there is a relation between the steady equilibrium flow